Available online at www.sciencedirect.com
SCIENCE DIRECT®
ELSEVIER
International Journal of Multiphase Flow 32 (2006) 51–81
International Journal of Multiphase Flow
www.elsevier.com/locate/ijmulflow

Counter-current gas–liquid flow in a vertical narrow channel—Liquid film characteristics and flooding phenomena

E.I.P. Drosos, S.V. Paras, A.J. Karabelas *

Department of Chemical Engineering, Aristotle University of Thessaloniki and Chemical Process Engineering Research Institute, University Box 455, GR 54 124 Thessaloniki, Greece

Received 14 April 2005; received in revised form 14 July 2005

Abstract

Results are reported of an experimental investigation of gas–liquid counter-current flow in a vertical rectangular channel with 10 mm gap, at rather short distances from liquid entry. Flooding experiments are carried out using air and various liquids (i.e., water, 1.5% and 2.5% aqueous butanol solutions) at liquid Reynolds numbers $Re_L < 350$. Visual observations and fast recordings suggest that the onset of flooding at *low* Re_L (<250) is associated with liquid entrainment from isolated waves, whereas "local bridging" is dominant at the *higher* Re_L examined in this study. Significant reduction of flooding velocities is observed with decreasing interfacial tension, as expected. Instantaneous *film thickness measurements* show that under conditions approaching flooding, a sharp increase of the mean film thickness, of mean wave amplitude and of the corresponding RMS values takes place. Film thickness power spectra provide evidence that by increasing gas flow the wave structure is significantly affected; e.g., the dominant wave frequency is drastically reduced. These data are complemented by similar statistical information from instantaneous *wall shear stress measurements* made with an electrochemical technique. Power spectra of film thickness and of shear stress display similarities indicative of the strong effect of waves on wall stress; additional evidence of the drastic changes in the liquid flow field near the wall due to the imposed gas flow, even at conditions below flooding, is provided by the RMS values of the wall stress. A simple model is presented for predicting the mean film thickness and mean wall shear stress under counter-current gas–liquid flow, below critical flooding velocities.
© 2005 Elsevier Ltd. All rights reserved.

* Corresponding author. Tel.: +30 2310 996201; fax: +30 2310 996209.
E-mail address: karabaj@cperi.certh.gr (A.J. Karabelas).

0301-9322/$ - see front matter © 2005 Elsevier Ltd. All rights reserved.
doi:10.1016/j.ijmultiphaseflow.2005.07.005

Keywords: Counter-current gas–liquid flow; Narrow vertical channel; Flooding; Film characteristics; Wall shear stress

1. Introduction

In recent years there is considerable interest in developing various types of compact devices such as two-phase *plate heat exchangers* and *compact reflux condensers*. In the latter, for example, the narrow flow passages between plates facilitate the onset of flooding that appears to be a limiting factor in their operation as it is associated with possible choking of the upward moving vapors and with a sharp rise of pressure drop. Therefore, it is important to determine the critical conditions leading to flooding in order to specify conditions of smooth condenser operation. Inadequate information on these issues exists in the literature, especially at *relatively small* Re_L and for rather *short plates*. Consequently, the purpose of this work is to study adiabatic gas–liquid counter-current flow, focusing on the onset of flooding, in a vertical rectangular channel with a rather narrow gap, at distances relatively close to liquid entry, thus simulating conditions of interest for the aforementioned applications.

In counter-current gas–liquid flow, the onset of flooding is identified by the critical gas flow rate at which partial liquid flow reversal is observed. Although flooding has been extensively studied in the past few decades, the amount of work for counter-current flow in *vertical rectangular channels* is limited, particularly for a narrow gap between the plates (Bankoff and Lee, 1986). The following brief survey is mainly concerned with counter-current flow inside rectangular channels, although a brief account of similar studies on flow inside vertical tubes is also provided. Lee and Bankoff (1984) conducted flooding tests at relatively large Re_L ($Re_L > 800$) in a rectangular channel for steam–water counter-current flow (where only one of the wider sides of the channel is wetted); their results clearly indicated the significant effect of the channel gap and inclination on flooding. Biage et al. (1989) studied experimentally the effect of gas flow on falling film characteristics for the case of air–water counter-current flow in a 250 mm wide vertical channel with a relatively large gap (25 mm), at $Re_L > 1500$; these tests showed that the onset of flooding is associated with droplet entrainment from standing waves. Roy and Jain (1989) measured the local thickness of a water film flowing down an inclined plane surface with counter-current gas flow, below critical flooding conditions, at various Re_L (ranging from 800 to 2000) focusing on the effect of inclination on film characteristics. A study of the dependence of flooding on duct geometry and inclination was presented by Zapke and Kroeger (2000a,b), at $Re_L > 400$, who additionally investigated the effect of fluid properties using several liquid and gas phases. Vlachos et al. (2001) reported flooding data for $Re_L > 200$ obtained in a vertical rectangular channel with 5 and 10 mm gap in a study of the effect of Re_L and channel gap on flooding mechanism.

Osakabe and Kawasaki (1989) conducted *top flooding* experiments in narrow rectangular passages of high aspect ratio (i.e., 10×100, 5×100 and 2×100 mm^2) at $Re_L > 400$. Their work was focused on the *partial delivery problem* (and not on *incipient* flooding), where the liquid downflow rate is different than the liquid feed rate and co-current upflow is observed to occur above the liquid entrance section. The flow system in that study, with a pool of liquid (of constant head) above the channel top, is quite different from the flow field studied here. Tests under similar (constant static head) liquid feeding conditions in vertical rectangular channels are reported by Larson

et al. (1994), Sudo et al. (1991) and Sudo (1996). Larson et al. (1994) studied the effect of location and geometry of the air injector on counter-current flow development inside very narrow rectangular channels of 1.1 and 2.2 mm gap. Sudo et al. (1991) and Sudo (1996) carried out experiments in channels of various dimensions (with duct gap and width 2.3–12.3 mm and 33–66 mm, respectively); they reported that the role of channel gap on flooding is very important, while no significant effect of the corresponding length was observed.

Dukler et al. (1984) and Zabaras (1985) studied the structure of the wavy interface on a falling film, at counter-current gas–liquid flow inside a 2 m long vertical tube, at various locations, for Re_L higher than 300, while Lacy and Dukler (1994) focused their study on the liquid feed region for the same range of Re_L. The results of these studies are subsequently compared with the present data, wherever is possible. Statistical film characteristics were obtained by Karimi and Kawaji (2000) in a vertical tube for air–kerosene counter-current annular flow at $Re_L > 1400$. Similar measurements for air–water annular flow were reported by Vijayan et al. (2001, 2002) who focused their study mainly on post-flooding conditions; the dependence of flooding mechanism on tube diameter was investigated as well. Recently, Mouza et al. (2002) studied flooding at $Re_L > 100$ in small diameter tubes (i.d. 6, 7, 8 and 9 mm) with air and two liquids (water and kerosene); the dominant flooding mechanism in almost all cases was found to be wave growth and upward dragging by the gas, initiated at the liquid exit. The strong effect of small tube diameter was evident in that study.

The above brief literature survey suggests that studies of vertical counter-current gas–liquid flow have been restricted to measurements of the time-averaged film thickness and of pressure drop at rather high Re_L ($Re_L > 1500$). Other detailed measurements such as instantaneous wall shear stress (not available for the geometry studied here), complementing liquid film thickness data could provide important insight into the problem at hand. An electrochemical technique was used by Wragg and Einarsson (1971) and Zabaras (1985) to investigate flow conditions at the wall in vertical counter-current flow in tubes. Wragg and Einarsson (1971) presented a rather large set of time-series of wall shear stress at various liquid and gas flow rates below critical flooding conditions, for Re_L between 40 and 1700. Their work, however, mainly dealt with the *qualitative* similarity between traces of the wall shear and of the corresponding film thickness. Zabaras (1985) made simultaneous measurements of film thickness and wall shear stress and investigated the influence of the imposed gas flow on the wall shear stress at two locations along the test tube (at distances 0.15 and 1.7 m from the liquid entry). Several studies of the hydrodynamic structure of rather thick films (at $Re_L > 1500$), in counter-current annular flow, are also reported for vertical tubes (e.g., Karimi and Kawaji, 1999, 2000), aimed at better understanding the effect of gas–liquid interaction on velocity distribution. It will be noted that in such studies, efforts to measure the velocity profile within the film were made; however, the wall shear stress was not measured directly but was estimated through the measured velocity profile.

In this paper, a description of the experimental equipment and procedures is presented first. Visual observations are reported next on the evolution of waves on falling films, providing a qualitative description of surface restructuring, due to counter-current gas flow, as well as an interpretation of the flooding data. Instantaneous local film thickness data as well as wall shear stress data and their statistical analysis are reported next. Finally, the data are interpreted and correlated.

2. Experimental setup and procedures

The experiments were carried out in a specifically designed and constructed experimental facility (Fig. 1a), the same one used to study *developing* free falling film characteristics (Drosos

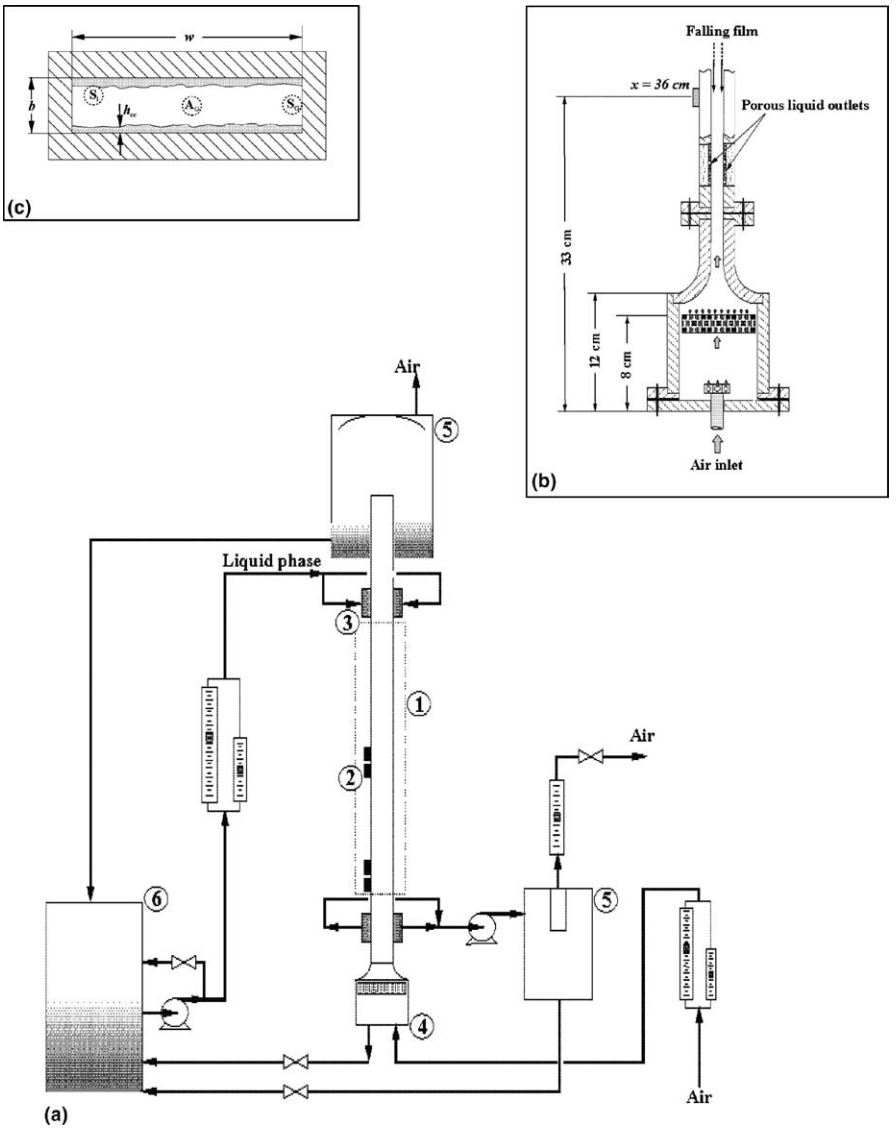

Fig. 1. (a) Schematic diagram of experimental flow loop: (1) cross-sectional view of the test section; (2) measurement stations-probes; (3) porous sections; (4) air entrance section; (5) phase separator; (6) liquid storage tank. (b) Detailed cross-sectional view of the air entrance section. (c) Cross-section of the channel.

et al., 2004). Two-phase flow is developed in a 70 cm high and 12 cm wide rectangular channel made of Plexiglas® to facilitate visual observations. The spacing between the two parallel plates is 10 mm and the active length of the test section is 38 cm. Air enters the device at the bottom through a specially made section (i.e., honeycomb) to achieve well-developed conditions before it contacts the falling liquid film. The liquid phase is introduced uniformly near the top of the channel and removed at the bottom through *porous sections*, made of stainless steel, with nominal pore size 100 μm (covering the entire active channel width) and embedded flush with the main flat surfaces in order to facilitate smooth liquid entry. Care is taken to uniformly feed the liquid and to minimize external disturbances upon film formation, by fixing a small liquid reservoir right behind each of the porous segments, which form one of the reservoir walls. The equipment arrangement provides a sufficiently long entry section for the gas (Fig. 1b) and minimizes the possibility of artificially creating disturbances at the liquid exit section.

2.1. Experimental conditions

The liquid and gas flow rates are measured by a bank of calibrated rotameters covering the range of the present experiments ($Q_L = 0.1$–0.7 l/min for the liquid phase and $Q_G = 6$–20 l/s for the air). In this work, Re_L is defined as

$$Re_L = \frac{4\Gamma_L}{\mu_L} \tag{1}$$

where Γ_L is the liquid mass flow rate per unit length of the plate and μ_L is the dynamic viscosity. A small amount of gas flows out, together with the liquid film removed in the lower porous section that varies between 10% and 15% of the gas inlet rate. The removed-gas flow rate is subtracted from that of the inlet gas in order to determine the true gas flow rate in the test section. On top of the measuring section there is a phase separator from which the liquid phase is fed back to the storage tank, whereas air is released to the atmosphere. Air and liquid are at ambient temperature (approx. 20 °C).

Before each set of experiments with water and butanol solution the inner surface of the Plexiglas® test section is cleaned by a dilute detergent solution and its wettability is improved by treating it with a *silica sol*. Such treatment is not necessary when an electrolytic solution is employed for shear stress measurements. This fluid is an aqueous solution of potassium ferri-cyanide (0.01 M) and potassium ferro-cyanide (0.05 M), with sodium hydroxide (1 M) used to suppress ionic migration effects. The ferri-cyanide diffusivity is obtained as proposed by Gordon et al. (1966). This solution is titrated prior to and after the experiments to determine the exact bulk concentration of ferri-cyanide ions. During the experiments the solution in the tank is preserved in a nitrogen atmosphere to prevent dissolvation of oxygen, whereas the Plexiglas® channel and all the other transparent sections of the experimental flow loop are covered by aluminum foil which protects the photo-sensitive electrolytic solution from light exposure. Apart from the electrolytic solution three liquids were also used, i.e., *water*, 1.5% and 2.5% w/w *aqueous n-butanol solutions*; liquid physical properties are listed in Table 1. The dilute butanol solutions were employed to obtain significantly smaller surface tension, with practically no effect on the density and viscosity, compared to water. The stability of the butanol solutions was checked prior to and after each

Table 1
Physical properties of the liquids used

	ρ_L, kg/m^3	μ_L, mPa s	σ, mN/m
Water	1000	1.00	75
1.5% butanol solution	995	1.03	50
2.5% butanol solution	980	1.09	40
Electrolytic solution	1080	1.25	42

experiment by measuring the surface tension and was found to be satisfactory (with an uncertainty of about 5%).

2.2. Film thickness measurements

The film thickness measurements were taken along the middle of the plate using the well-known "parallel-wire conductance technique" described elsewhere (e.g., Paras and Karabelas, 1991). Two probes (described by Drosos et al., 2004) were used, located in the lower half of the channel where incipient flooding is observed to occur, at distances from the liquid entry 19 cm and 36 cm. Two additional probes, at 22 cm and 33 cm from liquid entry (i.e., located 3 cm from the main probes) were employed to determine the celerity of surface waves.

2.3. Wall shear stress measurements

The local wall shear stress was measured using a well-known electrochemical technique (Reiss and Hanratty, 1962). The shear stress measurements were taken along the middle of the plate, at the same locations where film thickness was measured (i.e., at $x = 19$ and 36 cm); double (or "sandwich") probes were employed to determine both the magnitude and the direction of the wall shear stress. Each probe consists of two closely spaced parallel platinum strips 0.1 mm thick and approximately 4 mm wide, arranged normal to the main flow direction and mounted flush with the inner channel wall. One of the lower porous sections, having a much greater surface area than the probe (cathode), acts as the anode. The wall electrodes have to be calibrated in situ in vertical single-phase flow, to account mainly for imperfections of their surface. The calibration is carried out for each electrode prior to and after the main experiments.

Data sets of film thickness and liquid-to-wall shear stress are collected for a period of ~80 s (with a sampling frequency of 125 Hz) and a period of ~40 s (with a sampling frequency of 250 Hz), respectively.

2.4. Visual observations

Observations of the flow pattern at various locations along the plate were facilitated by fast video recordings, using a high speed camera (*Redlake Motion Scope PCI*®). The latter was aligned at two positions, one normal to the main plates and another (parallel to the plates) focusing inside the gap; a photoflood was used as a light source. A diffuser was placed in front of this source, to improve lighting of the main channel, aiming at better image quality of the growing waves.

3. Visual observations

Visualization experiments were carried out in order to study *qualitatively* the flow pattern during counter-current flow and to determine conditions associated with the onset of flooding. Each test started by first fixing the required liquid flow rate; next the gas flow rate was progressively increased stepwise until the onset of flooding. The latter is defined as *the condition where at least part of the liquid flow is reversed in direction and carried above the liquid entrance section, even in the form of droplets* (Hewitt, 1995).

The pictures in Fig. 2 are typical of liquid film development (near the liquid entrance) at various gas flow rates, including incipient flooding conditions. It is noted that these characteristics are qualitatively nearly the same for the three liquids employed. Film surface restructuring at this location—due to the gas–liquid interaction—seems to be more pronounced, even at the lower gas velocities examined in the present study, compared to that at the lower section of the channel (shown in Fig. 3). At small superficial gas velocity U_{GS}, i.e., far below critical conditions, there is an entrance length where the film surface appears to be smooth and undisturbed. Downstream nearly two-dimensional disturbances develop first, evolving into a three-dimensional, small-amplitude wave structure (e.g., Pierson and Whitaker, 1977; Chang, 1994; Drosos et al., 2004). By increasing the gas flow rate, the smooth entrance length is reduced and the initial small two-dimensional waves that appear near liquid entrance evolve rapidly into three-dimensional ones; furthermore, the film between the waves appears to be covered by smaller waves (ripples), having practically no undisturbed regions. As flooding is approached, the wavy disturbances on the film surface "move" upstream, covering the entire plate surface up to the liquid entry; additionally, the waves lose any feature of two-dimensionality. The effect of liquid flow rate is noticeable, if one compares pictures taken at $Re_L = 130$ and 225 (Fig. 2). At the entrance section, lower Re_L are associated with nearly two-dimensional waves over a larger range of gas flow rates (e.g., Fig. 2a, $U_{GS} = 6.5$ m/s). It should be noted that for the range of Re_L values and for all gas flow rates examined in this study ($U_{GS} < 11$ m/s) *no liquid reversal is observed* (by naked eye or detected in the recordings) to occur at this upper section of the channel. However, incipient flooding is observed in the *lower half* of the channel, mostly close to the *liquid exit area*, as shown in Fig. 3 where the influence of gas superficial velocity on wave structure is shown for the section between 22 and 32 cm from liquid entry. It appears that for low gas flow rates the wave structure at the lower half of the channel remains qualitatively nearly the same, close to the one corresponding to the free falling film case, as it has been also reported elsewhere for the case of counter-current flow in tubes far below the liquid entry (e.g., Mouza et al., 2002).

For conditions near the onset of flooding, notable features of the rather strong gas–liquid interaction are the fairly coherent large waves (like the one depicted in Fig. 3b for $U_{GS} = 7.5$ m/s, $t = 0$ ms) which seem to be momentarily arrested near the *liquid exit* by the counter-currently flowing gas. Such a wave, when formed, apparently cannot be transported (as a whole) upwards over a significant distance, but displays a tendency to become unstable and to eventually break up into droplets that follow the gas up-flow. It seems that most of these droplets are deposited on the surface of the falling film; only a small part appears to pass above the liquid injection station. After that event, the total liquid flow downwards is restored until a new wave is arrested near the exit and the process is repeated. The evolution of similar unstable, laterally coherent waves

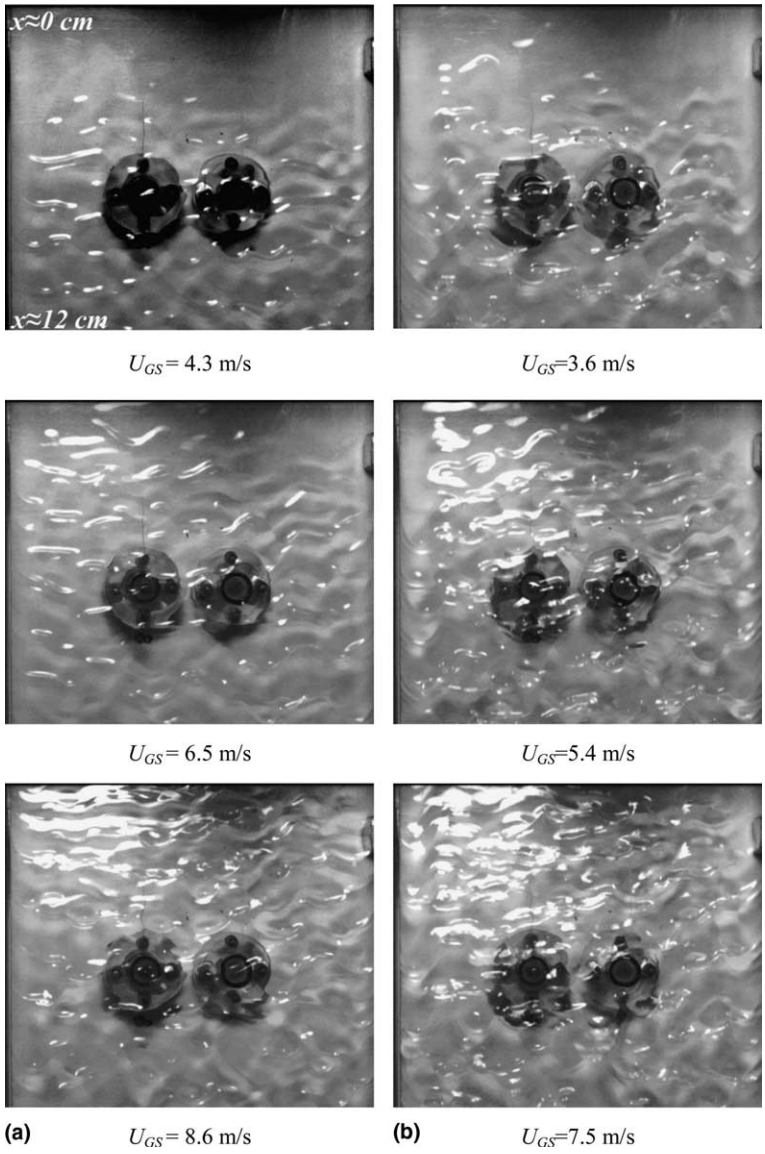

Fig. 2. Effect of gas velocity on liquid film flow on the channel main plate, at the entrance region ($x \approx 0$ to 12 cm), for 2.5% *butanol solution* at two *Reynolds* numbers: (a) $Re_L = 130$ and (b) $Re_L = 225$.

which appear intermittently near the exit has been also reported in the literature (e.g., Zabaras, 1985; Lacy and Dukler, 1994; Vijayan et al., 2001) for large Re_L ($Re_L > 1000$) and large diameter tubes ($D > 20$ cm); for the case of a rectangular channel with a rather large gap (25 mm), Biage et al. (1989) observed that some large waves did start moving upwards, but (almost immediately) "fell" downward and vanished. On the contrary Mouza et al. (2002) observed that the small tube diameter facilitates the development of (circumferentially) coherent waves which tend to grow and be dragged upward by the gas, at incipient flooding; the latter takes place at significantly smaller

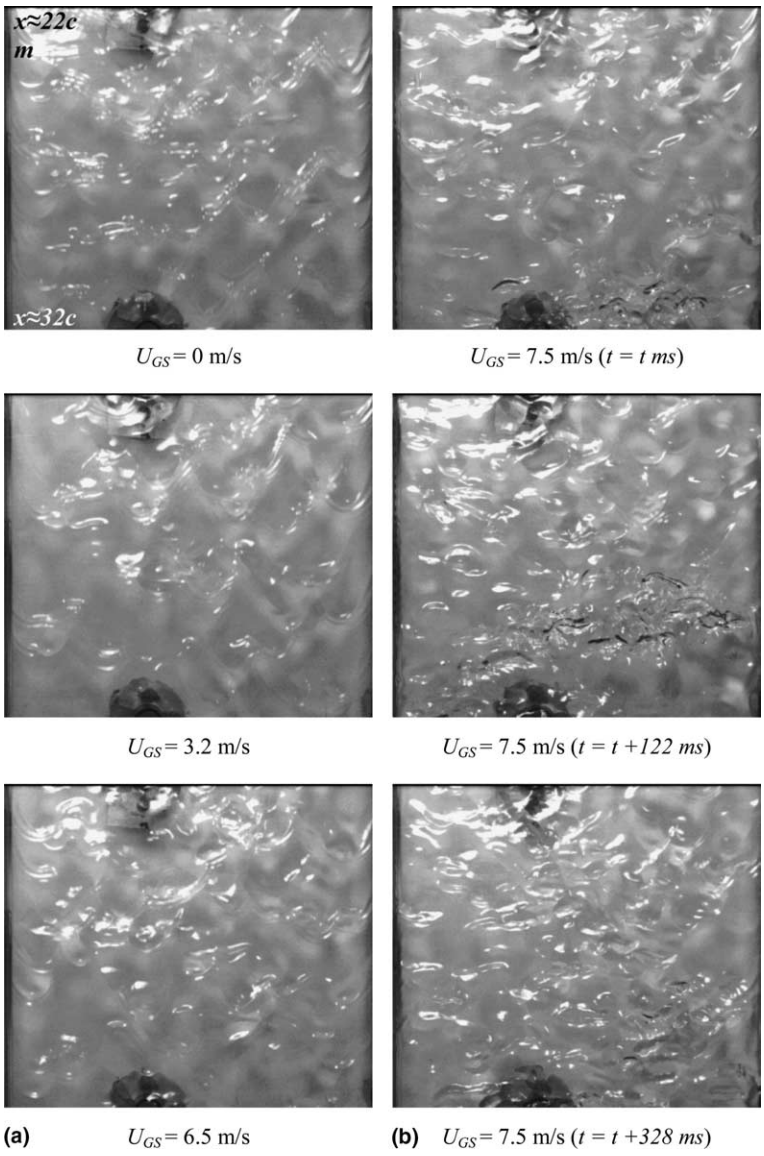

Fig. 3. Liquid film flow near the end of the channel for 2.5% *butanol solution* at $Re_L = 260$. (a) Flow pattern at various gas velocities. (b) Formation and disintegration of a coherent wave at flooding, over a period of 328 ms.

velocities than those observed in large size tubes, for the same range of Re_L (<350), and in the present study.

Interesting observations are made by focusing on the flow development inside the gap of the channel, between the two main plates, especially in the region near the liquid exit where the aforementioned coherent waves are formed. For $Re_L > 250$, it is clear that unstable waves (before breaking-up) tend to reach the wavy film on the opposite plate and to cause partial blockage of the gap (*local bridging*), due to the rapid increase of their amplitude. The liquid of these

"colliding" waves is forced by the gas to move upwards in the form of a slug, over some distance (less than about 10 cm) above the point where *bridging* is initially observed, until the gas eventually penetrates this slug leading to its disintegration. The largest portion of the liquid is then transported upwards (beyond the liquid inlet) in the form of rather large drops, while the remaining liquid seems to be dispersed in the lateral direction.

4. Critical flooding velocities

An overview of critical flooding conditions is provided in Fig. 4, for the three liquids tested, obtained by means of visual observations and fast video recordings. The data are plotted in terms of superficial gas velocity, $U_{GS} = \frac{Q_G}{wb}$ (Q_G, w and b are the volumetric gas flow rate, the channel width and gap respectively), at incipient flooding, vs. the corresponding Re_L; three main regions can be readily observed:

- *Region A*. This is the region of fairly strong dependence of critical flooding velocity on Re_L, where the superficial gas velocity is inversely proportional to Re_L. This trend is the usual one referred to in previously published studies (e.g., Hewitt, 1995; Bankoff and Lee, 1986).
- *Region B*. By further increasing the liquid flow rate in the range $Re_L \sim 150$–250, the flooding velocity tends to be weakly dependent on Re_L. Free falling film data for all three liquids examined (Drosos et al., 2004) may be used for a simple qualitative interpretation of this trend; these data show that the mean wave amplitude above the substrate, Δh_{mean}, at $Re_L \approx 150$–250 is roughly constant (as shown in Fig. 4 for the case of 2.5% butanol solution) which is in accord with the same trend of the flooding velocity.
- *Region C*. For $Re_L > 250$ a somewhat stronger dependence of critical velocity on Re_L is again evident. A plausible qualitative explanation may be based on the visual observations and the

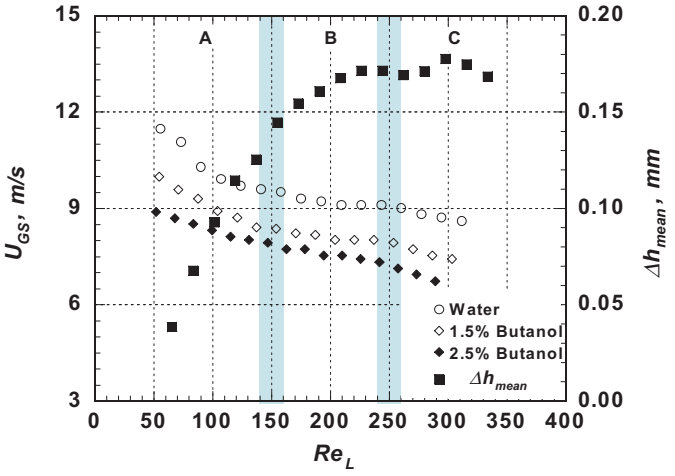

Fig. 4. Superficial gas velocity, U_{GS}, vs. Re_L (for the *three liquids* examined) at the onset of flooding, and mean wave amplitude Δh_{mean} for a free falling film of 2.5% *butanol solution* vs. Re_L at $x = 36$ cm (Drosos et al., 2004).

hydrodynamic analysis for the free falling film case (Drosos et al., 2004) indicating a more unstable flow with increasing Re_L; thus, the onset of flooding may be facilitated. This is consistent with the observed dominant mechanism for incipient flooding at $Re_L > 250$, which is characterized by wave growth and "local bridging". Furthermore, it is noted (Drosos et al., 2004) that the mean film thickness (in the absence of gas) continues to increase with Re_L in that range, even though the wave amplitude attains a nearly constant value. Therefore, a reduced free cross-sectional area is available for gas flow at $Re_L > 250$, requiring a smaller gas velocity for the initiation of flow reversal of the unstable liquid film.

The rather strong influence of the surface tension on flooding is evident in Fig. 4, the butanol solutions displaying lower critical velocities than water. This is a well-known trend (e.g., Bankoff and Lee, 1986; Zapke and Kroeger, 2000a,b; Mouza et al., 2002), attributed to the lower surface tension of butanol solutions which is associated with increased wave instability, as reported in the literature (e.g., Alekseenko et al., 1994), and already discussed in connection with free falling film data taken by Drosos et al. (2004) in the same channel. The influence of surface tension on wave growth and flooding is also shown and discussed in subsequently presented Figs. 8 and 9.

In Fig. 5 a comparison is shown of the present data for water with some published data for counter-current flow inside rectangular channels in terms of dimensionless velocities U_L^*, U_G^*. The channel gap, b, is adopted as the representative length scale for all data to facilitate comparison. The experimental results obtained by Mishima (1984), correspond to a rectangular channel

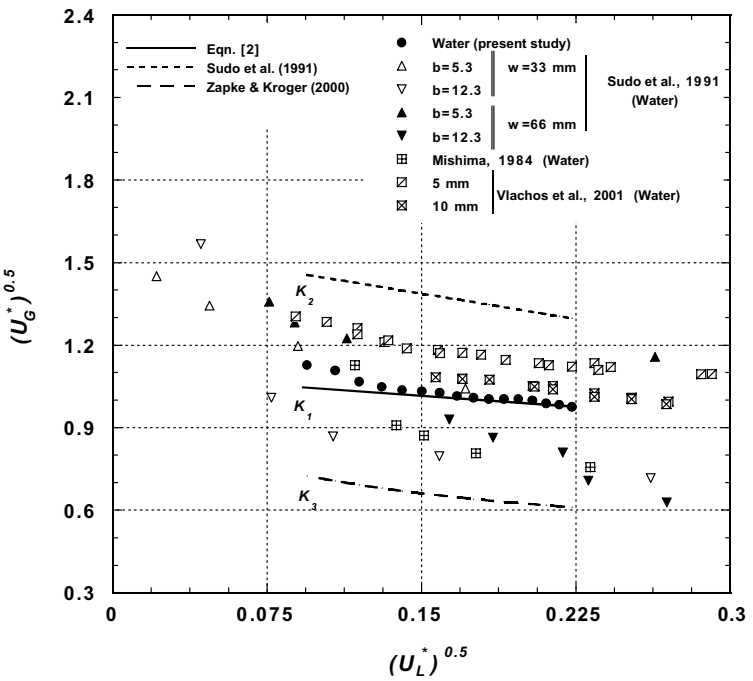

Fig. 5. Comparison of the present flooding data for *water* with literature experimental data, for rectangular channels, and with proposed empirical correlations.

having a width and a gap of 40 mm and 5 mm, respectively; these data are presented by Osakabe and Kawasaki (1989). Experimental results (of the present study and published ones in narrow rectangular channels) reveal that, at *very low* liquid flow rates, with decreasing U_L the critical gas velocity tends to increase quite sharply, whereas for the case of circular tubes at relatively high Re_L a linear increase is reported (e.g., Bankoff and Lee, 1986; Hewitt, 1995). The well-known Wallis (1969) correlation also involves a linear relation between:

$$U_L^* = U_{LS}\sqrt{\frac{\rho_L}{gb(\rho_L-\rho_G)}} \quad \text{and} \quad U_G^* = U_{GS}\sqrt{\frac{\rho_G}{gb(\rho_L-\rho_G)}}$$

Sudo et al. (1991) report that the aforementioned sharp increase is more pronounced when the ratio of channel width over its gap, w/b, decreases.

On the basis of their flooding velocities, Sudo et al. (1991) suggest that a Wallis-type expression for data correlation would be appropriate only at relatively large liquid flow rates, for which a linear dependence is observed between U_L^* and U_G^*. Such a correlation for the present data (for water), at the high liquid flow rates examined, is described by the following expression (marked as Line K_1 in Fig. 5):

$$\sqrt{U_G^*} + 0.708\sqrt{U_L^*} = 1.136 \tag{2}$$

The values of parameters C_1 (=0.708) and C_2 (=1.136) are greater than those proposed in the literature (e.g., Hewitt, 1995) but consistent with the trend reported by Sudo et al. (1991) showing that C_1 increases with both the width and the gap of the channel while C_2 increases with increasing width.

Fig. 5 also shows the estimated flooding velocities for conditions of the present study using again a Wallis-type expression (marked as Line K_2 in Fig. 5) for which the values of parameters C_1, C_2 are obtained from the empirical correlation proposed by Sudo et al. (1991):

$$C_1 = 0.5 + 0.0015Bo^{*1.3} \tag{3}$$

$$C_2 = 0.66\left(\frac{b}{w}\right)^{-0.25} \tag{4}$$

Here Bo^* is a modified *Bond* number defined as

$$Bo^* = \frac{wb(\rho_L-\rho_G)g}{\sigma} \tag{5}$$

where σ is the liquid surface tension.

The empirical correlation proposed by Zapke and Kroeger (2000a,b) is also included in Fig. 5 (marked as Line K_3):

$$U_G^* = \frac{0.0742}{U_L^* Oh_L^{0.15}} \tag{6}$$

where Oh_L is the *Ohnesorge* number defined as

$$Oh_L = \sqrt{\frac{\mu_L^2}{\rho_L b\sigma}} \tag{7}$$

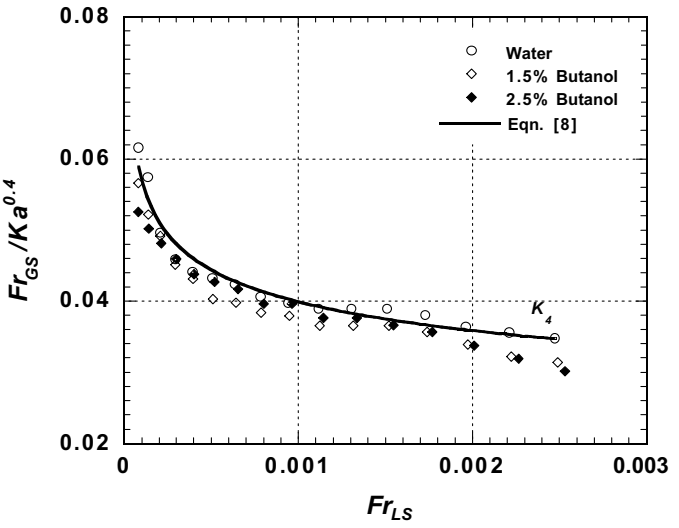

Fig. 6. Correlation of flooding conditions in dimensionless form, ($Fr_{GS}/Ka^{0.4}$) vs. Fr_{LS}, for the *three liquids* examined.

To obtain Line K_3 in Fig. 5, the Ohnesorge number was computed with water properties, to be compatible with the rest of the data.

These correlations deviate significantly from the present data, probably because the one proposed by Sudo et al. (1991) was obtained with smaller rectangular channels (i.e., with much greater values of U_L^*, between 0.25 and 1.5), while in Zapke and Kroeger (2000a,b) higher liquid flow rates where used, although flooding tests were conducted at channels of comparable dimensions with the present one.

In Fig. 6 an attempt is presented to relate the flooding data with the liquid physical properties by using the dimensionless gas Froude number, Fr_{GS}, (which is equal to U_G^{*2}) and liquid Kapitza, $K\alpha$, and Froude, Fr_{LS}, numbers. The data are correlated by the following expression:

$$Fr_{GS} = c_{fl} Ka^{0.4} Fr_{LS}^{-0.15} \tag{8}$$

where the constant $c_{fl} = 0.0138$ is used, and

$$Fr_{GS} = \frac{\rho_G U_{GS}^2}{gb(\rho_L - \rho_G)}, \quad Fr_{LS} = \frac{\rho_L U_{LS}^2}{gb(\rho_L - \rho_G)}, \quad Ka = \frac{\sigma}{\mu_L}\left(\frac{\rho_L}{\mu_L g}\right)^{1/3}$$

It is noteworthy that the critical flooding velocity is proportional to $Ka^{0.2}$ as Cetinbudaklar and Jameson (1969) obtained in their theoretical stability analysis.

5. Interpretation of instantaneous film thickness data

5.1. Film thickness characteristics

The study of the variation of film thickness variation with superficial gas velocity is focused on the lower half of the channel where initiation of flooding mainly occurs. Film thickness traces, not

presented here, clearly confirm the preceding qualitative visual observations. In Fig. 7 the variation of film thickness with superficial gas velocity is presented at $x = 19$ cm and $x = 36$ cm, for water and 2.5% butanol solution at various Re_L. Shaded areas in this and in subsequent graphs indicate approximately post-flooding conditions. It is evident that an increasing gas rate results in increasing mean thickness at both locations; this increase is rather small at low U_{GS}, but as the gas rate approaches the critical value for flooding, the mean thickness increases sharply. However, at $x = 19$ cm this trend appears to be less sharp, whereas at $x = 36$ cm the film thickness reaches a maximum value associated with the initiation of flooding which is mainly observed close to that location. Indeed, this maximum corresponds to the critical gas velocity obtained from visual observations (Fig. 4). Similar observations for the increase of film thickness with superficial gas velocity (but of smaller magnitude) are reported in the literature (Zabaras, 1985; Lacy and Dukler, 1994) for Re_L values greater than those of the present study. At large Re_L ($Re_L > 2000$), Biage et al. (1989), Karimi and Kawaji (2000) and Vijayan et al. (2002) report that the mean film

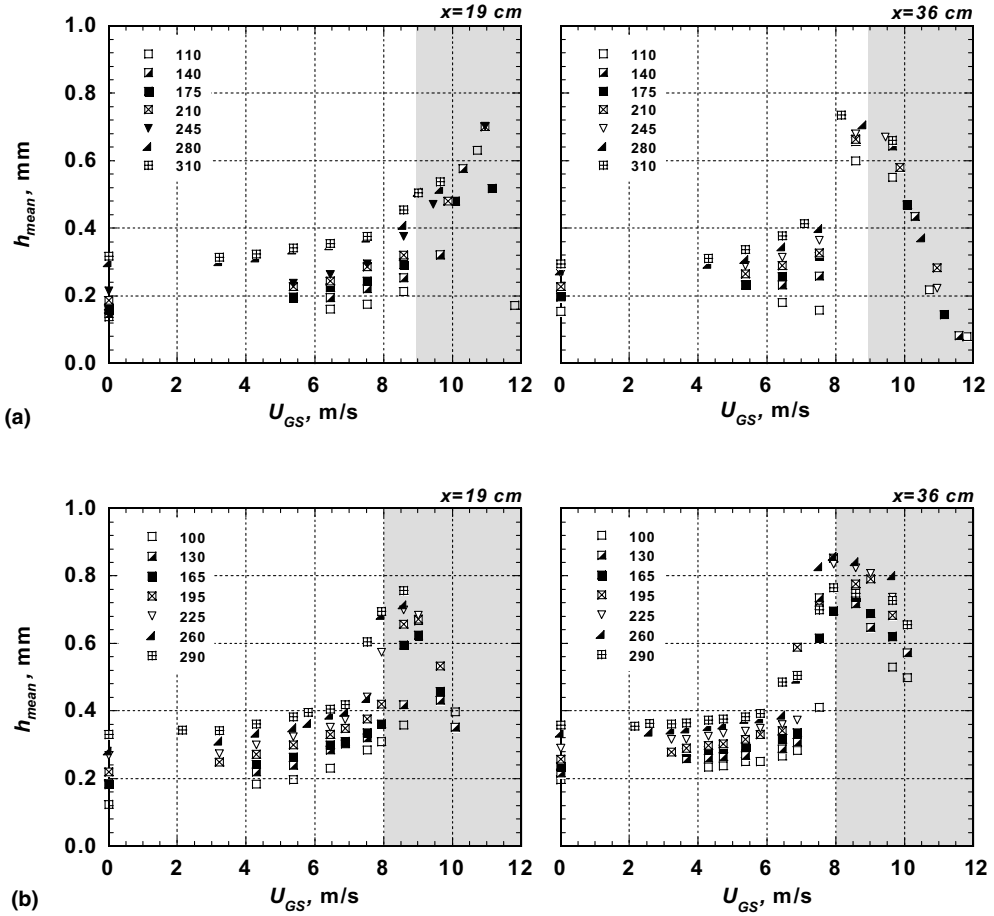

Fig. 7. Mean film thickness vs. U_{GS} for various Re_L at two locations along the test plate ($x = 19$ and 36 cm) for (a) *water* and (b) 2.5% *butanol solution*.

thickness displays a tendency of remaining constant, being almost independent of gas flow rate, up to the flooding point where a sharp increase is observed; a similar observation is reported by Zabaras (1985) for $Re_L > 1500$. It must be noted that (in the present tests) at the onset of flooding the measured *maximum* film thickness at $x = 36$ cm for $Re_L < 250$ is significantly lower compared to the length of the probe at that location (~2.7 mm), whereas for $Re_L > 250$, it is very close to this length. Therefore, the true mean film thickness at incipient flooding for $Re_L > 250$ may be larger than that measured with the present probes; the same is apparently true for the butanol solution (Fig. 7b).

Another parameter of the liquid film worth examining is the mean wave amplitude above the substrate, Δh_{mean}, and its variation with U_{GS}. This quantity is the mean value of the difference between a minimum in the film trace and the preceding maximum, corresponding to a large wave, for all large waves detected in a film thickness record (Drosos et al., 2004); the procedure for computing Δh_{mean} is reported elsewhere (Paras and Karabelas, 1991; Drosos et al., 2004). Fig. 8 shows

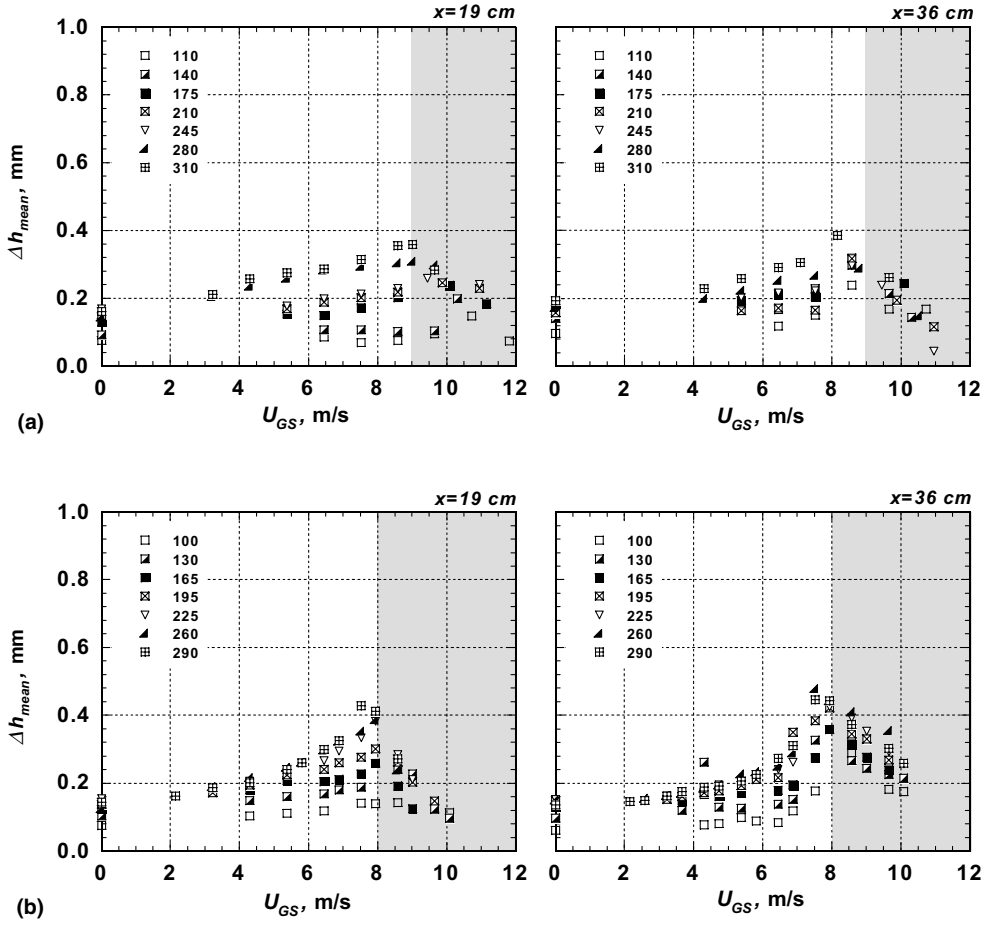

Fig. 8. Mean wave amplitude vs. U_{GS} for various Re_L at two locations along the test plate ($x = 19$ and 36 cm) for (a) *water* and (b) 2.5% *butanol solution*.

that the wave amplitude displays a trend similar to that of mean thickness, although in the latter case the increase near flooding is sharper. These trends for mean film thickness and wave amplitude suggest that a *substrate thickening* occurs with increasing U_{GS}; this was confirmed by determining the substrate thickness (not presented here due to space limitations).

The variation of RMS values of film thickness under counter-current flow, $h_{cc,RMS}$, plotted in Fig. 9 as a dimensionless RMS ratio (by dividing with the corresponding RMS values of film thickness at zero gas flow, $h_{ff,RMS}$) provides additional evidence of the change of wave structure; i.e., the roughness of the liquid film tends to grow as the gas flow rate increases. Near flooding there is a very sharp increase of h_{RMS} which is even sharper than that of mean thickness (Fig. 7). By further increasing the gas flow rate beyond critical conditions, it appears that $h_{cc,RMS}$, h_{mean}, and Δh_{mean} tend to decrease possibly due to the decreasing rate of liquid downflow, after partial liquid flow reversal.

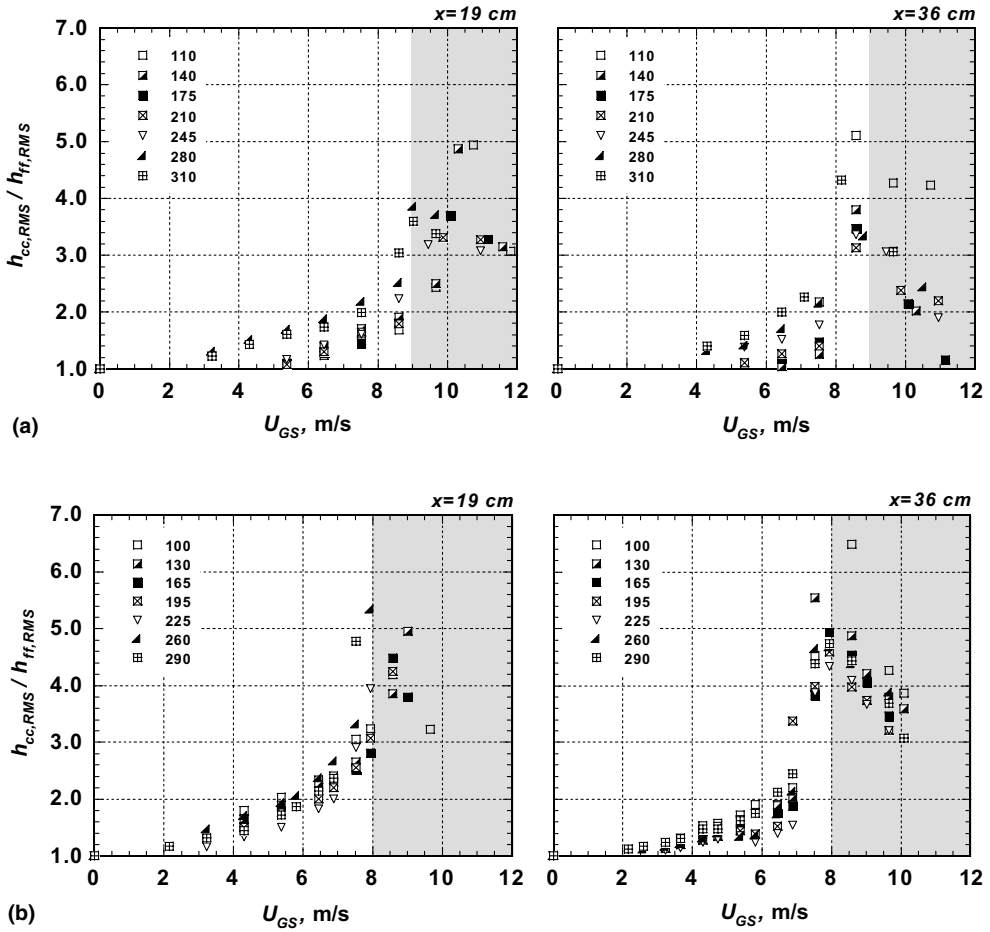

Fig. 9. Ratio of RMS values of film thickness at counter-current flow, over the corresponding RMS values at zero gas flow vs. U_{GS} for various Re_L at two locations along the test plate ($x = 19$ and 36 cm) for (a) *water* and (b) 2.5% *butanol solution*.

Interesting observations can be made by comparing the variation of liquid film characteristics (with U_{GS}) for the case of butanol solution to those for water (Figs. 7–9). For the lower surface tension solution it is evident that the critical gas velocity corresponds to the maximum value of mean film thickness at both locations; however this is not the case for water at $x = 19$ cm. This trend is attributed to the fact that the gas–liquid interaction results in a more disturbed interface for the butanol solution; this disturbance in the liquid film surface seems to be "uniformly" extending upwards, up to the liquid entry. A similar observation is reported by Zabaras (1985) for a low surface tension electrochemical solution used in his study. For water, the present data suggest that the film thickness at $x = 19$ cm continues to increase for conditions beyond flooding (Fig. 7a). The aforementioned difference between water and butanol solutions (due to different physical properties) also manifests itself in the larger values of h_{RMS} observed for the butanol solution at both locations and in the steeper increase of RMS values near the flooding point compared to those of water.

5.2. Power spectral density of film thickness fluctuations

Typical power spectral densities of film thickness for water and 2.5% butanol solution are shown in Fig. 10 for conditions near and at the flooding point (including the free falling film case) for the two locations along the channel, where the influence of the imposed gas flow on wave structure is reflected.

For the *free falling film* a pronounced maximum is observed at frequencies between 17 and 20 Hz at $x = 19$ cm, while at $x = 36$ cm this maximum corresponds to a frequency between 7 and 10 Hz; these frequencies are related to the periodic passage of large waves. For the case of low gas flow rates ($U_{GS} < 5$ m/s), it appears that the dominant wave frequency does not change significantly compared to the free falling film case; however, an increase of the energy conveyed by the waves is observed (especially for 2.5% butanol solution). This increase is more pronounced at higher gas flow rates towards flooding, along with the apparent reduction of the dominant frequency which at high U_{GS} lies roughly between 1 and 3 Hz. Such a reduction of the modal frequency is also reported by Zabaras (1985) and Biage et al. (1989); in their studies a dominant frequency of approx. 2–5 Hz was obtained at the onset of flooding. Another characteristic feature of the spectral density functions (Fig. 10) is a secondary frequency of approx. 3–5 Hz that seems to emerge at both measuring stations and may be attributed to a distribution of wave energy to smaller waves (possibly to *forerunner* waves located in front of larger ones) and their significant growth by further increasing gas flow rate. This secondary frequency eventually vanishes as flooding is approached. At rather high gas flow rates, an additional pronounced peak of approx. 10 Hz is observed in the spectrum corresponding to $x = 19$ cm for all liquids examined, especially at higher Re_L. This frequency may be indicative of a more "gradual" restructuring of the flow pattern at this location, with increasing U_{GS}, compared to the drastic changes that occur in the film flow near the liquid exit region; the latter are reflected in the rather sharp reduction of the modal frequency at $x = 36$ cm.

By further increasing gas flow rate above critical conditions, the dominant frequency remains nearly the same, but a decrease of the energy conveyed by the waves is evident possibly due to the decreasing rate of downflow.

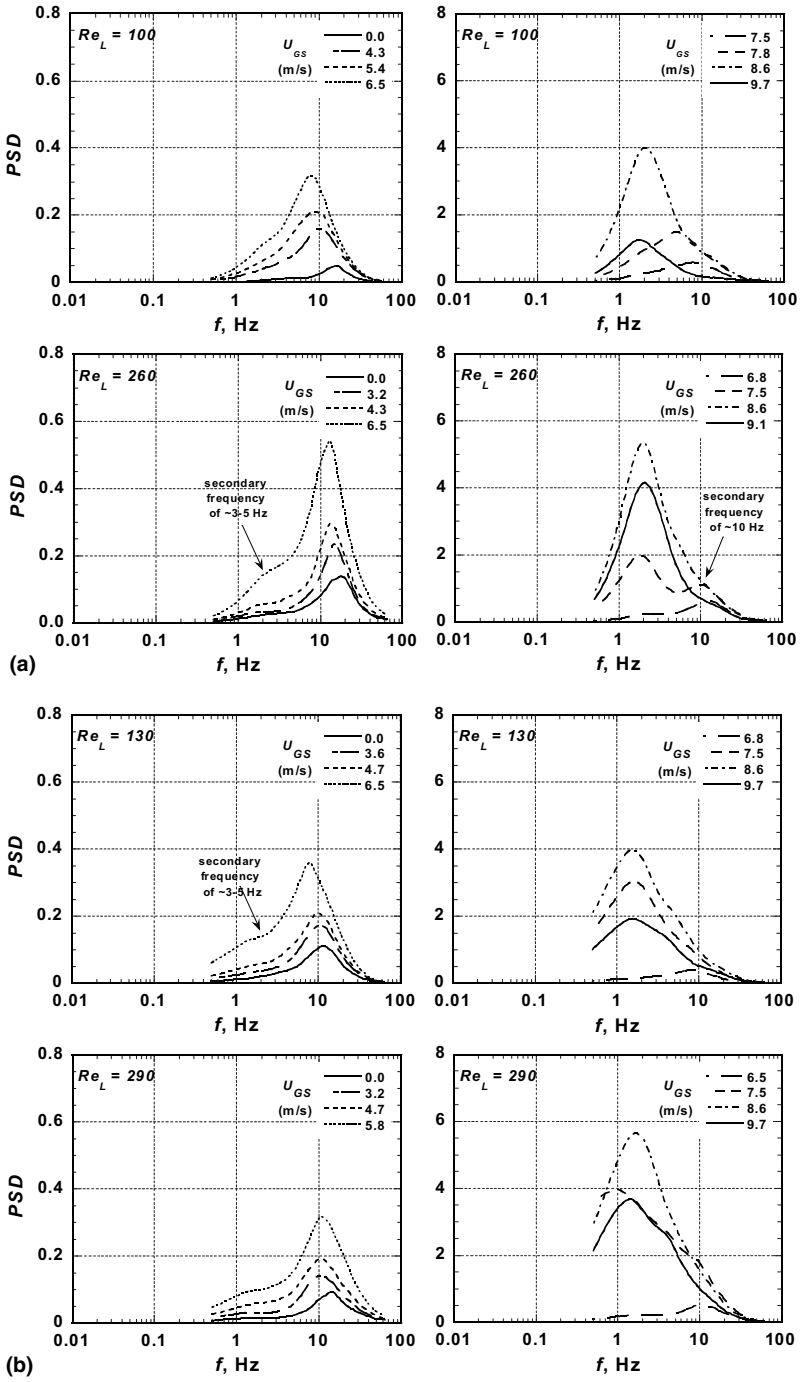

Fig. 10. Typical power spectral densities for 2.5% *butanol solution* for various Re_L and various U_{GS}, at two locations along the test plate: (a) $x = 19$ cm and (b) $x = 36$ cm.

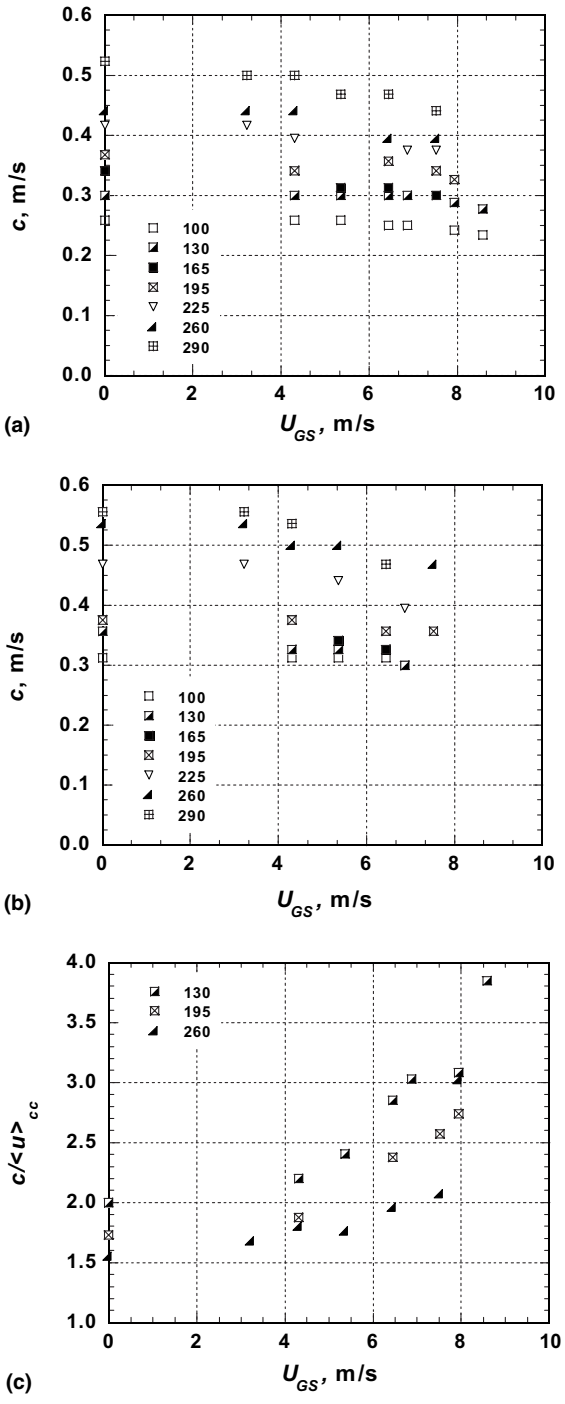

Fig. 11. Variation of wave celerity with U_{GS} for 2.5% *butanol solution*, for various Re_L, at two locations along the test plate: (a) $x = 19$ cm, (b) $x = 36$ cm, (c) $x = 19$ cm; wave celerity normalized with mean film velocity, $c/\langle u \rangle_{cc}$.

5.3. Wave celerity

Although a significant reduction of liquid wave celerity might have been expected on the basis of film flow retardation due to the interfacial shear stress, the present experimental results show that (at a given location) there is generally a rather modest reduction with increasing U_{GS}, even at high gas flow rates, whereas a somewhat stronger dependence on Re_L is observed (Fig. 11a, b). The rather small reduction of celerity with increasing U_{GS} may be related to the increase of the wave amplitude, in that the greater interfacial forces may be roughly counterbalanced by the increasing gravitational effect. Fig. 11c shows the normalized celerity $c/\langle u\rangle_{cc}$ data at $x = 19$ cm, where the mean film velocity $\langle u\rangle_{cc}$ is estimated on the basis of Eq. (A.8) using the measured thickness h_{mean}. It is interesting that wave celerity is much greater than $\langle u\rangle_{cc}$ well below flooding. The $c/\langle u\rangle_{cc}$ data at $U_{GS} = 0$ display the trend already discussed by Drosos et al. (2004).

It is worth mentioning that near flooding, a chaotic flow pattern prevails, resulting in a poor correlation; therefore, it is not possible to obtain a reliable estimate of wave celerity through a cross-correlation function at such high gas velocities. A nearly constant wave celerity is also reported by Zabaras (1985) and Biage et al. (1989); in these studies it is noticed that the large waves which are correlated well enough for $Re_L > 700$ (even at the onset of flooding) continue to travel downwards without being decelerated. In the study by Karimi and Kawaji (2000) at high Re_L (>2000) a significant reduction of surface velocity was noticed only for gas flow rates beyond flooding.

6. Interpretation of instantaneous wall shear stress data

6.1. Mean and RMS wall shear stress

The purpose of the measurements was to determine both the direction and the magnitude of the wall stress. The flow direction of the falling film near the wall was found to be downward at all gas rates examined; i.e., changes of the wall shear stress sign did not appear to occur.

Typical shear stress traces at $x = 19$ cm and 36 cm are depicted in Fig. 12 providing an indication of the surface structure influence on wall shear stress fluctuations. The sharp peaks in both cases may be attributed to the gas–liquid interface waves which seem to affect local velocity and shear stress at the channel wall. A notable feature of these time-series is the increase of the amplitude of shear stress fluctuations with gas velocity at both locations; however, it seems that the flow pattern in the proximity to the wall is influenced less by surface waves at location $x = 19$ cm (especially at low gas flow rates) than at $x = 36$ cm; i.e., near the liquid exit. Apparently, waves of somewhat smaller amplitude (at $x = 19$ cm) have reduced influence on local velocities at the wall. A similar trend is also reported in previous studies (Zabaras, 1985; Karimi and Kawaji, 1999; Moran et al., 2002), where it is shown that the substrate film surrounding a wave structure is strongly influenced mainly by the presence of large-amplitude waves, whereas in the region of developing flow the growing waves cannot exert their influence down to the wall.

The time series of wall shear stress data are statistically analyzed to obtain the time-averaged wall shear stress, $\tau_{w,mean}$, and the corresponding root mean square, $\tau_{w,RMS}$. The variation of

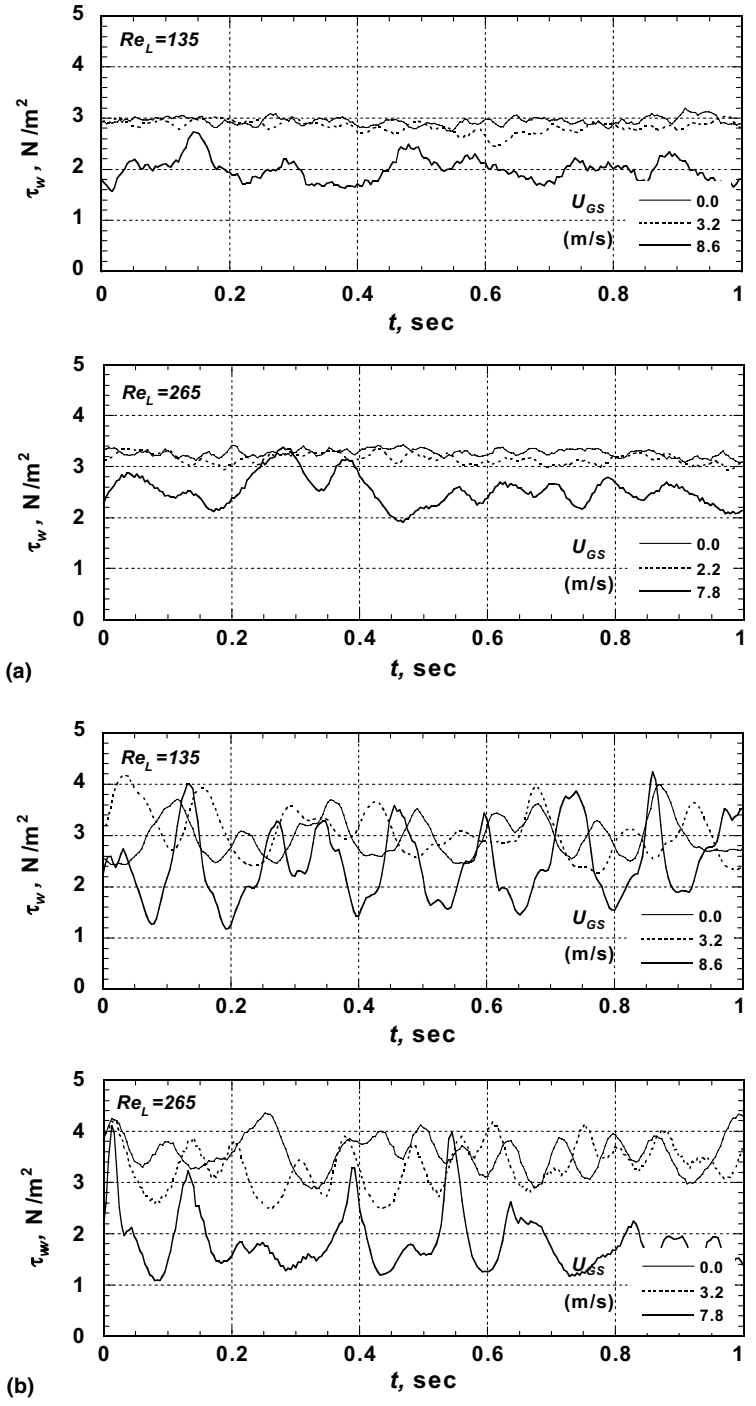

Fig. 12. Typical traces of wall shear stress taken simultaneously for two Re_L ($Re_L = 135$ and 265) and various U_{GS}, at two locations along the test plate: (a) $x = 19$ cm and (b) $x = 36$ cm.

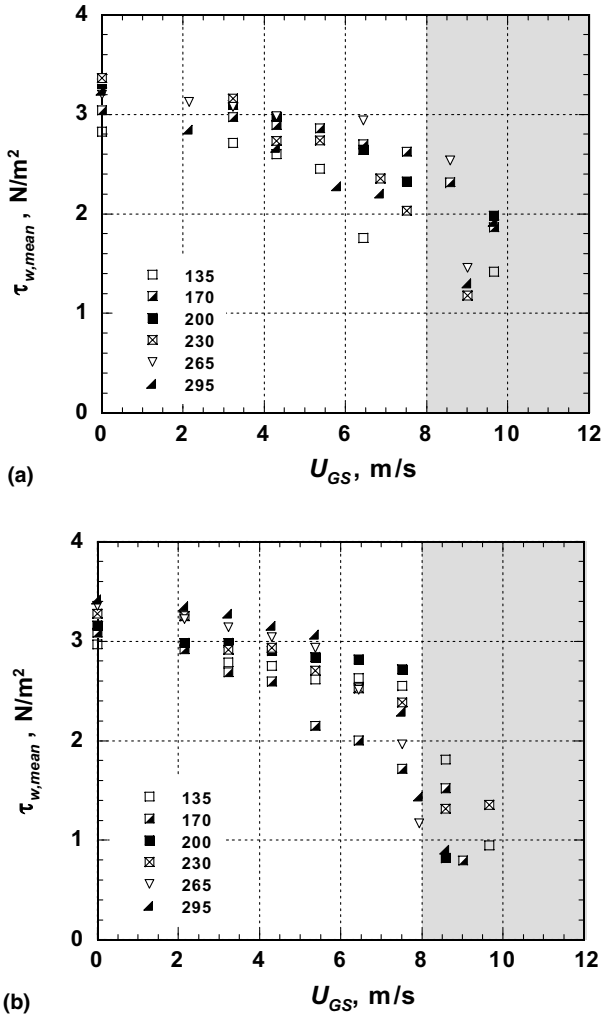

Fig. 13. Mean wall shear stress $\tau_{w,mean}$ vs. U_{GS} for various Re_L at two locations along the test plate: (a) $x = 19$ cm and (b) $x = 36$ cm.

$\tau_{w,mean}$ with superficial gas velocity, for various Re_L, is presented in Fig. 13. Increasing gas flow rate results in decreasing wall stress since the gravity force acting on the liquid is partially counterbalanced by the gas–liquid interfacial shear as well as by wall shear forces. By further increasing gas velocity above ~6–7 m/s the flooding point is approached, and a sharp reduction of the mean shear stress is observed. This trend is quite similar to the sharp increase displayed by the mean film thickness and mean wave amplitude, indicating that the influence of interfacial gas–liquid shear extends down to the solid wall. Additional support of this observation is provided by the RMS values of shear stress (Fig. 14) which display a tendency to increase with increasing gas velocity, as also noticed by Zabaras (1985) and Karimi and Kawaji (1999). The RMS values reach a maximum at the flooding point; this trend is apparently related to the more disturbed surface structure observed at higher gas flow rates, reflected also in the RMS values of film thickness (Fig. 9).

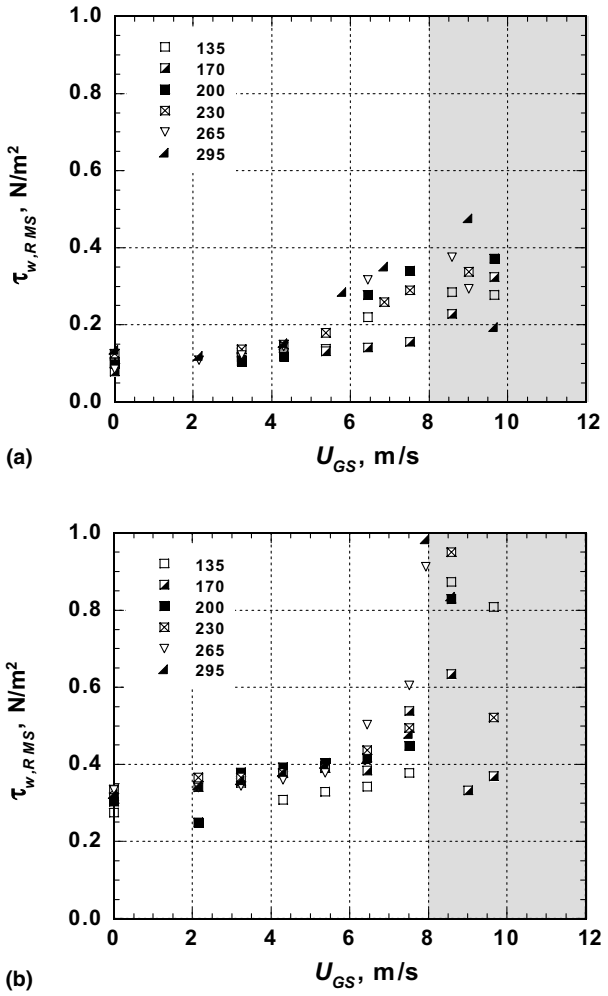

Fig. 14. RMS values of mean wall stress vs. U_{GS} for various Re_L at two locations along the test plate: (a) $x = 19$ cm and (b) $x = 36$ cm.

6.2. Power spectral density of wall shear stress fluctuations

The influence of the interfacial wave structure on the flow pattern near the wall is also examined via typical power spectral density functions of wall shear stress fluctuations, depicted in Fig. 15 for three different values of Re_L, corresponding to a location near the liquid exit ($x = 36$ cm) where the surface structure seems to be better developed than at the upper or at the middle section of the channel. A distinct peak, at frequencies between 7 and 10 Hz, is evident for the *free falling film* case. This dominant frequency seems to be independent of liquid flow rate (Re_L), in contrast to the observed reduction of its value when gas flow rate increases; at conditions near flooding the modal frequency reaches a value between 2 and 4 Hz. A similar trend is reported by Wragg and Einarsson (1971) and Zabaras (1985). Another notable feature of the spectral density functions in Fig. 15

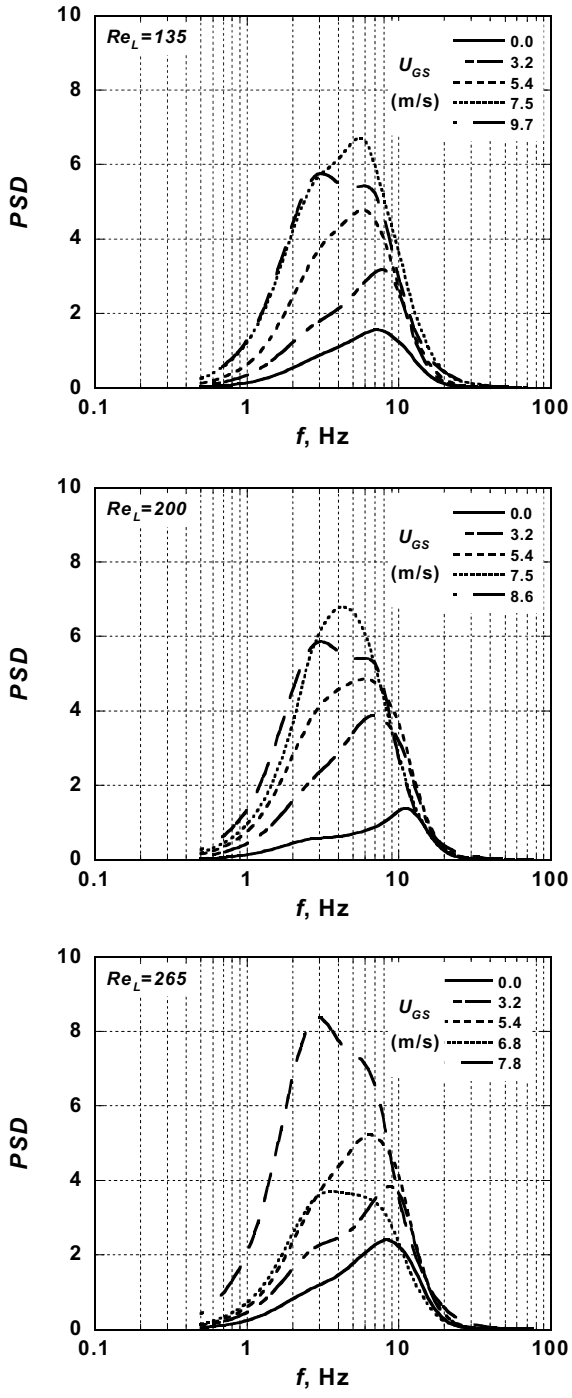

Fig. 15. Typical power spectral densities of wall shear stress fluctuations at counter-current flow for various Re_L at $x = 36$ cm.

is the apparent increase of the maximum (peak) value with increasing gas flow rate. An additional frequency peak at approx. 3–5 Hz seems to emerge as gas flow rate increases (especially at higher Re_L) and may be attributed to the significant growth of the smaller waves that influence the flow field close to the wall.

It is clear that the spectral density functions of shear stress and liquid film thickness are very similar indicating the influence of waves on film flow. It should be pointed out, however, that this similarity does not imply that instantaneous shear stress is in-phase with film thickness; the present data, not taken simultaneously, cannot resolve this issue. According to Zabaras (1985), where simultaneous measurements of film thickness and shear stress were made, the correlation between these two quantities improves as the distance of the measuring station, below liquid feed, increases, whereas it is very poor at a region close to that of wave inception. For the latter region a better correlation is established only at rather high gas flow rates.

6.3. Film thickness—wall shear stress interrelationship

The present experimental results reveal that even at rather high gas velocities, just below the flooding point, the film flow is dominated by the downward wave motion. Furthermore, it appears that there is a rather insignificant net effect of imposed gas flow on wave celerity up to about flooding conditions; indeed it seems that wave celerities are nearly equal to the ones corresponding to zero gas flow for the same liquid rate (Fig. 11). However, the effect of the interfacial shear on film flow is not negligible; counter-current gas flow strongly affects all the other wave characteristics and it is associated with drastic liquid film restructuring.

In Appendix A, a simple model is presented to estimate the average film thickness at counter-current flow, h_{cc}, and the mean wall shear stress, $\tau_{w,mean}$, at U_{GS} below the onset of flooding. For

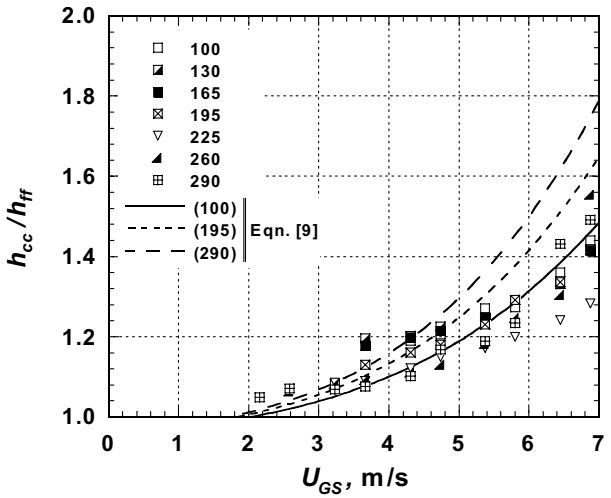

Fig. 16. Comparison of the present experimental results plotted as h_{cc}/h_{ff} vs. U_{GS} for 2.5% *butanol solution* at $x = 36$ cm with predictions based on Eq. (9). Predictions correspond to Re_L values of 100, 195 and 290.

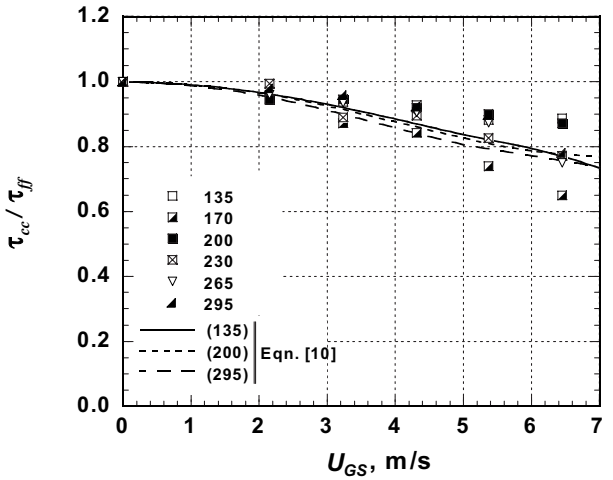

Fig. 17. Comparison of the present experimental results plotted as τ_{cc}/τ_{ff} vs. U_{GS} for the *electrolytic solution* at $x = 36$ cm with predictions based on Eq. (10). Predictions correspond to Re_L values of 135, 200 and 295.

steady, one-dimensional film flow with imposed shear, τ_i, at the gas–liquid interface, these quantities may be calculated from the following expressions:

$$\frac{(\rho_L-\rho_G)g-\frac{2}{w}\tau_G-\frac{2}{\alpha_r b}\tau_i}{\rho_L g}\left(\frac{h_{cc}}{h_{ff}}\right)^3-\frac{3}{2}\frac{\tau_i}{\rho_L g h_{ff}}\left(\frac{h_{cc}}{h_{ff}}\right)^2-1=0 \tag{9}$$

$$\tau_{w,mean}=\mu_L\left.\frac{dU_x}{dy}\right|_{y=0}=\left(\rho_L g-\rho_G g-\frac{2}{w}\tau_G-\frac{2}{\alpha_r b}\tau_i\right)h_{cc}-\tau_i \tag{10}$$

Fig. 16 displays the predicted variation of the ratio of the mean film thickness at counter-current flow over the mean thickness for the free falling film case, h_{cc}/h_{ff}, with superficial gas velocity U_{GS} for the case of 2.5% butanol solution; the experimental results are also included. In Fig. 17 a similar comparison is shown of the estimated wall shear stress at counter-current flow normalized with wall stress for the laminar flow case (at zero gas flow), τ_{cc}/τ_{ff}, with the experimental results taken at $x = 36$ cm. In both comparisons, fair agreement is obtained between predictions and experimental data with a maximum uncertainty 15% at the higher U_{GS} examined. Thus, Eqs. (9) and (10) may be used for the prediction of mean film thickness and wall shear at counter-current flow for given gas and liquid flow rates.

7. Concluding remarks

It is observed that incipient flooding takes place mainly close to the liquid exit of the rather short test-section employed. The onset of flooding at Re_L smaller than 250 is associated with growth, flow reversal (momentarily) and disintegration of waves covering part of the film surface in the lateral direction; liquid droplets torn-off those waves are entrained by the gas. At higher Re_L (>250), local "bridging" of surface waves is the dominant mechanism. The wave structure of the

free falling film, on which gas shearing is applied, tends to influence to a great extent wave evolution (at increasing U_{GS}) and flooding.

Instantaneous film thickness and wall shear stress measurements were made at two locations at the lower half of the channel. By increasing the gas flow rate a relatively small increase of mean film thickness, h_{mean}, and of mean wave amplitude, Δh_{mean}, is observed well below the critical flooding velocity, compared to the rather sharp increase of these quantities near the onset of flooding. The effect of gas velocity appears to be comparatively stronger on the RMS values of film thickness which tend to increase significantly even at gas flow rates well below the flooding point. Flooding transition corresponds to a distinct change in the form of the power spectrum and it is associated with a significant reduction of the dominant wave frequency. Furthermore, the energy conveyed by the waves is increasing with increasing Re_L or U_{GS}.

The wall shear stress measurements show no evidence of liquid film flow reversal up to the onset of flooding. The observed reduction of mean wall shear with increasing gas flow rate may be attributed to the increased gas–liquid interfacial shear caused by the increase of the mean wave amplitude. The increasing RMS values of wall shear stress fluctuations, with increasing gas rate, are in accord with a similar increase displayed by the RMS of instantaneous film thickness and is indicative of the influence of interfacial waves on flow close to the wall. At relatively low gas velocities ($U_{GS} < 5$ m/s) this wave effect is found to be more pronounced near the liquid exit (i.e., at $x = 36$ cm), whereas flow at the wall is almost unaffected by waves at locations closer to the liquid entry (i.e., at $x = 19$ cm). Additional evidence on the influence of large waves on liquid flow at the wall is provided by the similarities between the film thickness and wall shear power spectra.

In general, the falling film characteristics obtained in this study show that significant changes occur in liquid film flow, even close to the channel wall, under conditions approaching flooding. The proposed simple model for predicting the mean wall shear stress and mean film thickness (below the onset of flooding) provides only first estimates. To complement the present data and develop reliable predictive tools for flooding, additional work is required on flow in narrow passages. The effects of gap size/shape and of liquid properties need special attention.

Acknowledgement

The authors wish to thank Mr. A. Lekkas, Mr. T. Tsilipiras and Mr. F. Lambropoulos for the technical support.

Appendix A. A model to estimate mean film thickness and mean wall shear stress in counter-current gas–liquid flow

Assuming steady, laminar one-dimensional flow subject to interfacial shear one obtains:

$$-\frac{1}{\rho_L}\left(\frac{dp}{dx}\right) + g + \frac{\mu_L}{\rho_L}\frac{d^2U_x}{dy^2} = 0 \tag{A.1}$$

with boundary conditions

$$U_x = 0 \qquad \text{at } y = 0$$
$$\left.\frac{\mathrm{d}U_x}{\mathrm{d}y}\right|_{y=h_{cc}} = -\frac{\tau_i}{\mu_L} \qquad \text{at } y = h_{cc}$$

The origin of coordinates is placed at the channel wall; y is the distance from the wall and x is the axial coordinate.

Integration of (A.1) yields:

$$\tau_{yx} = \mu_L \frac{\mathrm{d}U_x}{\mathrm{d}y} = \left(\rho_L g - \frac{\mathrm{d}p}{\mathrm{d}x}\right)(h_{cc} - y) - \tau_i \tag{A.2}$$

For counter-current flow in a vertical rectangular channel in which only the wide plates are considered to be wetted by the falling film, a force balance in the gas "core" gives:

$$-\frac{\mathrm{d}p}{\mathrm{d}x}A_G + \rho_G g A_G + \tau_G S_G + \tau_i S_i = 0 \tag{A.3}$$

where A_G, S_G and S_i are defined in Fig. 1c. The fluctuation at the gas–liquid interface is neglected and Eq. (A.3) leads to

$$-\frac{\mathrm{d}p}{\mathrm{d}x} + \rho_G g + \frac{2}{w}\tau_G + \frac{2}{\alpha_r b}\tau_i = 0 \tag{A.4}$$

where α_r is the void fraction in a given section of the channel:

$$\alpha_r = \frac{b - 2h_{cc}}{b} \tag{A.5}$$

Substitution of Eq. (A.4) in Eq. (A.2) leads to an expression for the shear stress distribution:

$$\tau_{yx} = \mu_L \frac{\mathrm{d}U_x}{\mathrm{d}y} = \left(\rho_L g - \rho_G g - \frac{2}{w}\tau_G - \frac{2}{\alpha_r b}\tau_i\right)(h_{cc} - y) - \tau_i \tag{A.6}$$

The velocity distribution is obtained by integrating Eq. (A.6):

$$U_x(y) = \frac{\left(\rho_L g - \rho_G g - \frac{2}{w}\tau_G - \frac{2}{\alpha_r b}\tau_i\right)}{\mu_L}\left(h_{cc}y - \frac{y^2}{2}\right) - \frac{\tau_i}{\mu_L}y \tag{A.7}$$

while the liquid flow rate, per unit width of the channel, may be obtained as

$$Q = \int_0^{h_{cc}} U_x(y)\,\mathrm{d}y = \frac{\left(\rho_L g - \rho_G g - \frac{2}{w}\tau_G - \frac{2}{\alpha_r b}\tau_i\right)}{3\mu_L}h_{cc}^3 - \frac{\tau_i}{2\mu_L}h_{cc}^2 \tag{A.8}$$

In the absence of gas flow, Eq. (A.8) is reduced to

$$Q = \frac{\rho_L g h_{ff}^3}{3\mu_L} \tag{A.9}$$

where h_{ff} is the mean thickness for the case of the free falling film.

Given that this analysis is restricted to counter-current flow below critical conditions, Q is considered constant independent of gas flow rate; dividing Eq. (A.8) by (A.9) leads to

$$1 = \frac{(\rho_L - \rho_G)g - \frac{2}{w}\tau_G - \frac{2}{\alpha_r b}\tau_i}{\rho_L g}\left(\frac{h_{cc}}{h_{ff}}\right)^3 - \frac{3}{2}\frac{\tau_i}{\rho_L g h_{ff}}\left(\frac{h_{cc}}{h_{ff}}\right)^2 \tag{A.10}$$

The mean wall shear stress, $\tau_{w,mean}$, is obtained from Eq. (A.6) for $y = 0$:

$$\tau_{w,mean} = \mu_L \left.\frac{dU_x}{dy}\right|_{y=0} = \left(\rho_L g - \rho_G g - \frac{2}{w}\tau_G - \frac{2}{\alpha_r b}\tau_i\right)h_{cc} - \tau_i \tag{A.11}$$

In the above expressions, the gas wall shear stress, τ_G, is given in terms of a friction factor, f_G, and the superficial gas velocity, U_{GS}; i.e.,

$$\tau_G = \frac{1}{2} f_G \rho_G U_{GS}^2 \tag{A.12}$$

where

$$f_G = 0.079 Re_{GS}^{-0.25} \tag{A.13}$$

and

$$Re_{GS} = \frac{U_{GS} b \rho_G}{\mu_G} \tag{A.14}$$

The interfacial shear stress is expressed in terms of an interfacial friction factor, f_i, as follows:

$$\tau_i = \frac{1}{2} f_i \rho_G U_{GS}^2 \tag{A.15}$$

Here it is assumed that the superficial gas velocity is much greater than the liquid surface velocity which is neglected. To the authors' best knowledge, there are no data available on the value of interfacial shear stress in counter-current flow inside a vertical rectangular channel. In order to obtain an independent estimate of interfacial friction factor, f_i, the following modified empirical correlation—originally proposed by Bharathan et al. (1979)—presented by Sudo (1996) for the case of counter-current flow inside a vertical rectangular channel, may be employed:

$$f_i = 0.008\left[1 + C_3\left(\frac{h_{cc}}{D_e}\right)^{C_4}\right] \tag{A.16}$$

where D_e is the equivalent hydraulic diameter of the channel ($D_e \approx 2b$) and the parameters C_3, C_4 are defined as follows. Here, the value of h_N (obtained from the well-known *Nusselt* formula; $h_N = \left(\frac{3\Gamma_L \mu_L}{\rho_L^2 g}\right)^{1/3} = \left(\frac{3}{4}\frac{\mu_L^2}{\rho_L^2 g}\right)^{1/3} Re_L^{1/3}$) is used for convenience, instead of h_{ff}.

$$C_3 = 41.3 Bo_e^{(C_4+0.25)} 10^{9.07/Bo_e} \tag{A.17}$$

$$C_4 = 1.63 + \frac{4.74}{Bo_e} \tag{A.18}$$

and Bo_e is the Bond number based on D_e:

$$Bo_e = D_e \left[\frac{(\rho_L - \rho_G)g}{\sigma} \right]^{1/2} \tag{A.19}$$

References

Alekseenko, S.V., Nakoryakov, V.E., Pokusaev, B.G., 1994. Wave Flow of Liquid Films. Beggel House Inc., New York.

Bankoff, S.G., Lee, S.C., 1986. A critical review of the flooding literature. In: Hewitt, G.F., Delhaye, J.M., Zuber, N. (Eds.), Multiphase Science and Technology. Hemisphere, New York, pp. 95–180, Chapter 2.

Bharathan, D., Wallis, G.B., Richter, H.J., 1979. Air–water counter-current two-phase flow. EPRI Rep. No. NP-1165.

Biage, M., Delhaye, J.M., Vernier, Ph., 1989. The flooding transition: a detailed experimental investigation of the liquid film before the flooding point. ANS Proceedings, National Heat Transfer Conference, ANS, pp. 53–60.

Cetinbudaklar, A.G., Jameson, G.J., 1969. The mechanism of flooding in vertical counter-current two-phase flow. Chem. Eng. Sci. 24, 1669–1680.

Chang, H.-C., 1994. Wave evolution on a falling film. Annu. Rev. Fluid Mech. 26, 103–136.

Drosos, E.I.P., Paras, S.V., Karabelas, A.J., 2004. Characteristics of developing free falling films at intermediate Reynolds and high Kapitza numbers. Int. J. Multiphase Flow 30, 853–876.

Dukler, A.E., Smith, L., Chopra, A., 1984. Flooding and upward film flow in tubes—I: Experimental studies. Int. J. Multiphase Flow 10, 585–597.

Gordon, S.L., Newman, J.S., Tobias, C.W., 1966. The role of ionic migration in electrolytic mass transport: diffusivities of $[Fe(CN_6)]^{3-}$ and $[Fe(CN_6)]^{4-}$ in KOH and NaOH solutions. Ber. Bunsenges. Phys. Chem. 70, 414–420.

Hewitt, G.F., 1995. In search of two-phase flow. 30th US National Heat Transfer Conference, Portland, Oregon.

Karimi, G., Kawaji, M., 1999. Flow characteristics and circulatory motion in wavy falling films with and without counter-current gas flow. Int. J. Multiphase Flow 25, 1305–1319.

Karimi, G., Kawaji, M., 2000. Flooding in vertical counter-current annular flow. Nucl. Eng. Des. 200, 95–105.

Lacy, C.E., Dukler, A.E., 1994. Flooding in vertical tubes—I: Experimental studies of the entry region. Int. J. Multiphase Flow 20, 219–233.

Larson, T.K., Oh, C.H., Chapman, J.C., 1994. Flooding in a thin rectangular slit geometry representative of ATR fuel assembly side-plate flow channels. Nucl. Eng. Des. 152, 277–285.

Lee, S.C., Bankoff, S.G., 1984. Parametric effects on the onset of flooding in flat-plate geometries. Int. J. Heat Mass Transfer 27, 1691–1700.

Mishima, K., 1984. Boiling burnout at low flow rate and low pressure conditions. Ph.D. Thesis, Research Reactor Institute, Kyoto University, Japan cited by Osakabe, M., Kawasaki, Y., 1989. Top flooding in thin rectangular and annular passages. Int. J. Multiphase Flow 15, 747–754.

Moran, K., Inumaru, J., Kawaji, M., 2002. Instantaneous hydrodynamics of a laminar wavy liquid film. Int. J. Multiphase Flow 28, 731–755.

Mouza, A.A., Paras, S.V., Karabelas, A.J., 2002. The influence of small tube diameter on falling film and flooding phenomena. Int. J. Multiphase Flow 28, 1311–1331.

Osakabe, M., Kawasaki, Y., 1989. Top flooding in thin rectangular and annular passages. Int. J. Multiphase Flow 15, 747–754.

Paras, S.V., Karabelas, A.J., 1991. Properties of the liquid layer in horizontal annular flow. Int. J. Multiphase Flow 17, 439–454.

Pierson, F.W., Whitaker, S., 1977. Some theoretical and experimental observations of the wave structure of falling liquid films. Ind. Eng. Chem. Fund. 18, 401–408.

Reiss, L.P., Hanratty, T.J., 1962. Measurement of instantaneous rates of mass transfer to a small sink on a wall. AIChE J. 8, 245–247.

Roy, R.P., Jain, S., 1989. A study of thin water film flow down an inclined plate without and with counter-current flow. Exp. Fluids 7, 318–328.

Sudo, Y., 1996. Mechanism and effects of predominant parameters regarding limitation of falling water in vertical counter-current two-phase flow. J. Heat Transfer (Trans. ASME) 118, 715–724.

Sudo, Y., Usui, T., Kaminaga, M., 1991. Experimental study of falling water limitation under a counter-current flow in a vertical rectangular channel (first report, effect of flow channel configuration and introduction of CCFL correlation). JSME Int. J., Series II, 34, 169–174.

Vijayan, M., Jayanti, S., Balakrishnan, A.R., 2001. Effect of tube diameter on flooding. Int. J. Multiphase Flow 27, 797–816.

Vijayan, M., Jayanti, S., Balakrishnan, A.R., 2002. Experimental study of air–water counter-current annular flow under post-flooding conditions. Int. J. Multiphase Flow 28, 51–67.

Vlachos, N.A., Paras, S.V., Mouza, A.A., Karabelas, A.J., 2001. Visual observations of flooding in narrow rectangular channels. Int. J. Multiphase Flow 27, 1415–1430.

Wallis, G.B., 1969. One Dimensional Two-phase Flow. McGraw-Hill, New York.

Wragg, A.A., Einarsson, A., 1971. Instantaneous local rates of liquid–solid mass transfer in a rippling film: the effect of co- and counter-current gas flow. Chem. Eng. Sci. 26, 1289–1292.

Zabaras, G.J., 1985. Studies of vertical annular gas–liquid flows. Ph.D. Thesis, University of Houston, USA.

Zapke, A., Kroeger, D.G., 2000a. Counter-current gas–liquid flow in inclined and vertical ducts—I: Flow patterns, pressure drop characteristics and flooding. Int. J. Multiphase Flow 26, 1439–1455.

Zapke, A., Kroeger, D.G., 2000b. Counter-current gas–liquid flow in inclined and vertical ducts—II: The validity of the Froude–Ohnesorge number correlation for flooding. Int. J. Multiphase Flow 26, 1457–1468.